Journal of Materials Science: Materials in Electronics
https://doi.org/10.1007/s10854-018-0112-z

Simultaneously excellent upconversion luminescence and temperature sensing properties in tungstate multiphase phosphors

Ying Zhang[1,2,3] · Xusheng Wang[1] · Huihua Ye[1] · Xue Gong[1] · Yongxiang Li[2] · Xi Yao[1]

Received: 10 August 2018 / Accepted: 24 September 2018

Abstract
For optical temperature sensor, high luminescence intensity is as important as high temperature sensing sensitivity. In this work, research on rare-earth ions Er^{3+}/Yb^{3+} codoped $KY(WO_4)_2$–K_2WO_4 multiphase phosphors for optical temperature sensing application was first proposed by material design. Under a 980 nm excitation, the upconversion luminescence intensity of multiphase materials was much higher than that of pure phase materials. For the 0.6KYW–0.4KW multiphase material, excellent temperature sensing property that the maximal sensitivity was 14.7×10^{-3} K^{-1} at 643 K in a broad temperature range from 83 to 663 K was simultaneously obtained. These results indicate that $KY(WO_4)_2$–K_2WO_4 multiphase phosphors with excellent upconversion luminescence and temperature sensing properties are promising candidates for optical temperature sensors.

1 Introduction

Temperature is an important physical quantity, which can be measured in many different approaches [1–5]. As one advanced temperature measurement, optical temperature sensor based on the fluorescence intensity ratio (FIR) technique has many advantages [3, 6–13], compared with conventional methods of temperature measurements. It could be used in many harsh environments, such as power stations, oil refineries, coal mines, etc. without interference from outside environment [14–17]. For optical temperature sensor, high temperature sensing sensitivity (S) is of crucial importance. In practical use, wide temperature range, stability of S and high luminescence intensity in operating temperature range are very valuable.

It is known that, the properties of materials are determined by their composition and structures. Tungstate, known to be excellent sensitizer for rare earth luminescence, has been widely studied as phosphors and scintillators, especially as effective hosts for optical temperature sensing because of their chemical stability, relatively low phonon energy and the self-activating ability [18, 19]. For rare earth ions Y^{3+}, Gd^{3+}, La^{3+} and Lu^{3+}, their ionic radius and chemical properties of are similar to that of activators and sensitizers ion. Most of their inorganic compounds are suitable for upconversion luminescence (UCL) matrix materials [20–28]. For example, $NaY(WO_4)_2$, $NaGd(WO_4)_2$ and $KY(WO_4)_2$ tungstate materials are used as solid laser materials [29], which makes them very good matrix materials. It is found that fairly high S has been realized by co-doping Er^{3+} and Yb^{3+} ions in tungstate-based hosts, such as $CaWO_4$, $SrWO_4$, $ZnWO_4$, $MgWO_4$ and $NaY(WO_4)_2$ [3, 14, 15, 17, 30–33]. However, for many phosphors, the increase of temperature is not favorable for luminescence, while boosting excitation power of laser can significantly improve it, but high excitation power may have a heating effect on sample [14, 31, 34–36]. To avoid the heating effect on samples, the UCL intensities of tungstate materials above at a lower excitation power are not high enough. In the testing process, both low luminescence intensity and change of excitation

✉ Xusheng Wang
xs-wang@tongji.edu.cn

✉ Yongxiang Li
yxli@mail.sic.ac.cn

[1] Functional Materials Research Laboratory, School of Materials Science and Engineering, Tongji University, 4800 Cao'an Road, Shanghai 201804, China

[2] The Key Laboratory of Inorganic Functional Materials and Devices, Shanghai Institute of Ceramics, Chinese Academy of Sciences, Shanghai 200050, China

[3] University of Chinese Academy of Sciences, Beijing 100049, China

Published online: 27 September 2018

power could lead to inaccurate measurement. Therefore, our primary aim is to look for the phosphors which has a high luminescence intensity in low excitation power.

Along with the progress of materials science, materials can be designed according to the requirement. Multiphase material shows its unique performance by assembling the advantage of each single-phase material, which provides a broader consideration for material design. In our previous study on strontium tungstate phosphors, it was found that the UCL property of strontium tungstate multiphase materials outdistanced that of pure strontium tungstate materials [14]. This implies us an idea that by material design the multiphase phosphors with excellent UCL and temperature sensing properties could be obtained. Potassium tungstate-based multiphase materials were selected as the target materials because of their physical performances and chemical stability.

In this study, we prepared the Er^{3+}/Yb^{3+} codoped $KY(WO_4)_2$–K_2WO_4 multiphase phosphors by material design. It is expected to improve the UCL property by modifying the matrix materials. The UCL property and optical temperature sensing performance in a temperature range from 83 to 663 K of Er^{3+}/Yb^{3+} codoped $KY(WO_4)_2$–K_2WO_4 multiphase phosphors are presented. Largely enhanced UCL intensity and excellent temperature sensing behavior indicate that Er^{3+}/Yb^{3+} codoped $KY(WO_4)_2$–K_2WO_4 multiphase phosphors have great potential applications in optical temperature sensors.

2 Experimental

Er^{3+}/Yb^{3+} codoped $KY(WO_4)_2$–K_2WO_4 multiphase phosphors were designed as $xKY(WO_4)_2$–$(1-x)$ K_2WO_4 (x = 0, 0.3, 0.6, 0.8,1 .0) and synthesized by a solid-state reaction method, the samples denoted as xKYW–(1 − x) KW. In order to study the effect of different matrix materials on the UCL performance, the concentration of Er^{3+} and Yb^{3+} are 1 mol% and 10 mol% respectively. Stoichiometric amounts of raw materials K_2CO_3 (99.9%), WO_3 (99.8%), Y_2O_3 (99.99%), Er_2O_3 (99.9%) and Yb_2O_3 (99.9%) were thoroughly mixed in ethanol. The homogeneous mixture was then calcined at 700–800 °C for 2 h in a muffle furnace. After calcination, 10 wt% polyvinyl alcohol (PVA) binder was uniformly added into the reground powders. Then they were pressed into disk-shaped pellets of 10 mm in diameter and 2 mm in thickness. Finally, samples were sintered at temperatures of 800–900 °C for 2 h in an alumina crucible in air.

The structure phase of the samples was analyzed using an X-ray diffractometer (XRD, Bruker D8 Advanced, Germany) with Cu Kα1 radiation (λ = 0.154056 nm), tube voltage 40 kV, and tube current 40 mA, in 2θ angle ranging from 10° to 70° at room temperature, with a scanning speed of 5 °/min. UCL spectra were obtained using a 980 nm laser diode (HJZ980-100) to excite the surface of samples. The photons emitted from sample were detected by a fluorescence spectrophotometer (F-7000, Hitachi High-Technologies Corporation, Tokyo, Japan). The laser beam was coupled into an optical fiber, collimated and then focused to sample. For temperature sensing measurement, the sample was placed on a heating stage controlled by a TP94 temperature

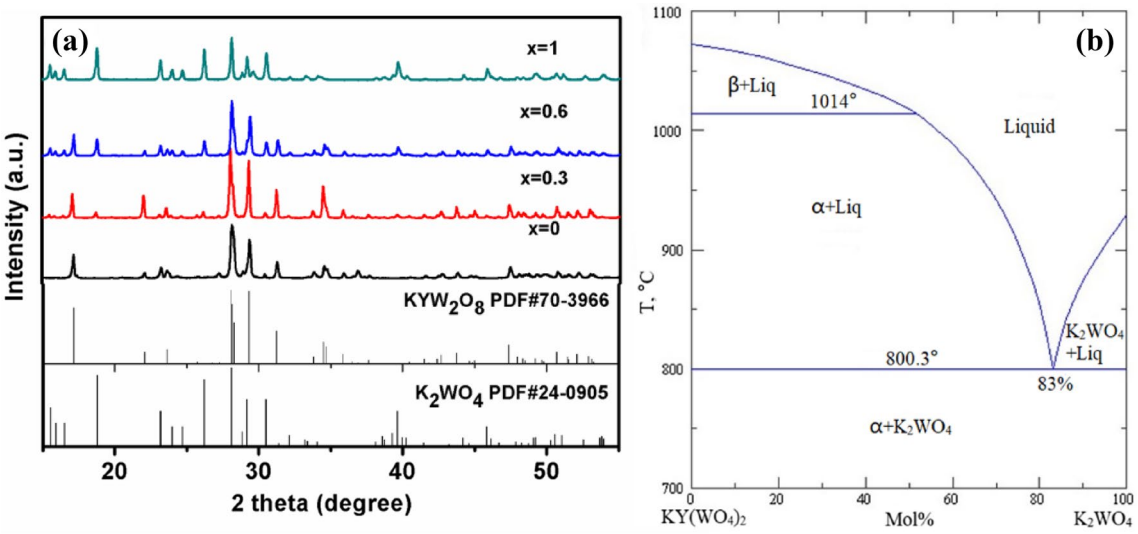

Fig. 1 **a** XRD patterns of xKYW–(1 − x) KW samples. The standard data for KYW_2O_8 and K_2WO_4 are shown as the reference. **b** Binary phase diagram of $KY(WO_4)_2$–K_2WO_4 system, α and β represent low-temperature $KY(WO_4)_2$ and high-temperature $KY(WO_4)_2$ phase

Table 1 The crystal phase composition of xKYW–(1 – x) KW samples

x	Phase
0	K_2WO_4
0.3	$KY(WO_4)_2 + K_2WO_4$
0.6	$KY(WO_4)_2 + K_2WO_4$
1	$KY(WO_4)_2$

controller (Linkam Scientific Instruments Ltd, Surrey, UK) with a heating rate of 10 K/min. All samples are of the same thickness to ensure the accuracy of the measurement.

3 Results and discussion

From the XRD pattern of xKYW–(1 – x) KW phosphors (Fig. 1a), the samples (x = 0 and 1) exhibit pure K_2WO_4 and $KY(WO_4)_2$ monoclinic crystal phase and no secondary impure phase is observed. For 0.3KYW–0.7KW sample, the secondary phase $KY(WO_4)_2$ coexists with K_2WO_4 phase, whereas, for 0.6KYW–0.4KW sample, the secondary phase K_2WO_4 coexists with $KY(WO_4)_2$ phase. This can be explained by the binary phase diagram of $KY(WO_4)_2$–K_2WO_4 system in Fig. 1b. From the binary phase diagram, a eutectic point (800 °C) exists in the $KY(WO_4)_2$ and K_2WO_4 system. Above melting point temperature, $KY(WO_4)_2$ and K_2WO_4 become completely miscible and form a single homogeneous system. When temperature drops, $KY(WO_4)_2$ and K_2WO_4 phases crystallized separately from the liquid phase. Therefore, the samples (0 < x < 1) are multiphase materials with both $KY(WO_4)_2$ and K_2WO_4 phases. The crystal phase composition of xKYW–(1 – x) KW samples are listed in Table 1.

Under a 980 nm excitation, the xKYW–(1 – x) KW samples exhibit very unusual UCL spectrum shapes at room temperature, as shown in Fig. 2a. For all samples, the baseline drifts up and down in the whole wavelength range. For multiphase samples, the UCL spectra are composed of three bands, two strong green emission bands from the thermally coupled energy levels ($^2H_{11/2}$, $^4S_{3/2}$) to

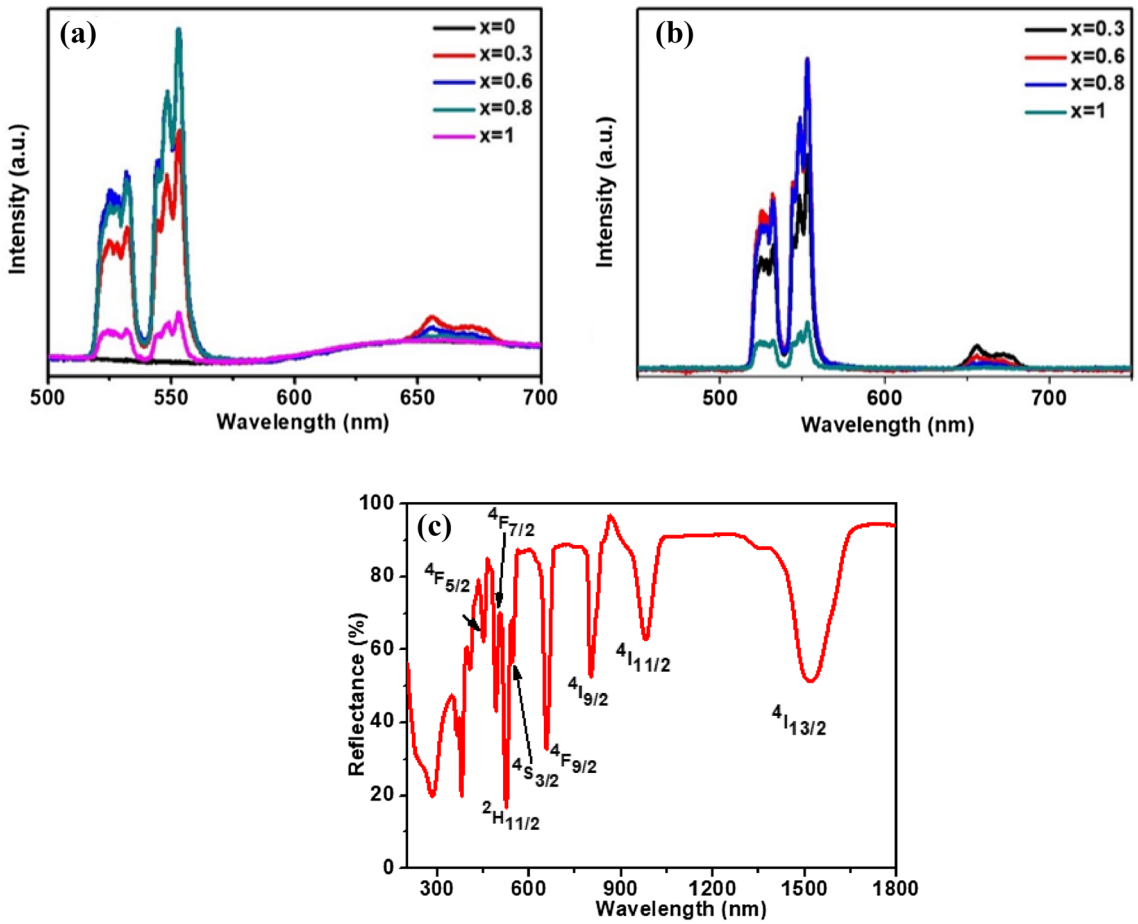

Fig. 2 **a** The UCL spectra of xKYW–(1 – x) KW samples; **b** the common background method dealing with the background of xKYW–(1 – x) KW samples, the UCL spectra of pure KW sample is treated as the background; **c** reflectance spectrums of KYW sample in the wavelength region from 200 to 1800 nm at room temperature

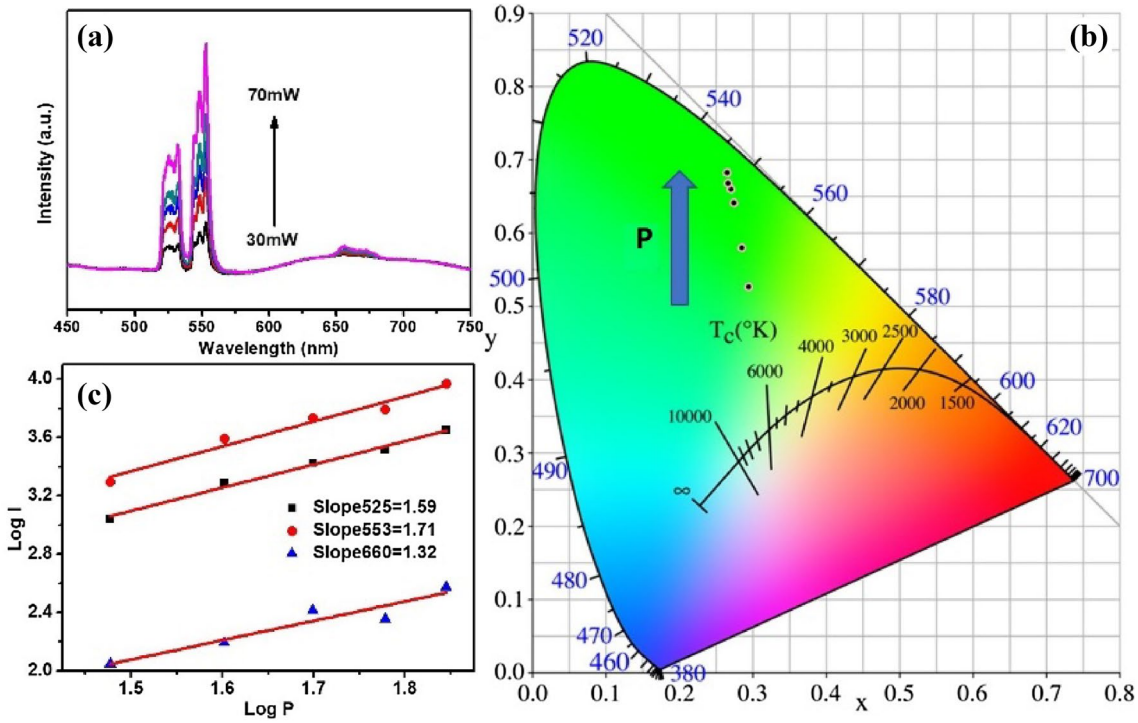

Fig. 3 **a** The UCL spectra, **b** CIE chromaticity diagram of UC emissions and **c** Log I versus Log P plot for 0.6KYW–0.4KW sample under different pump power from 30 to 70 mW

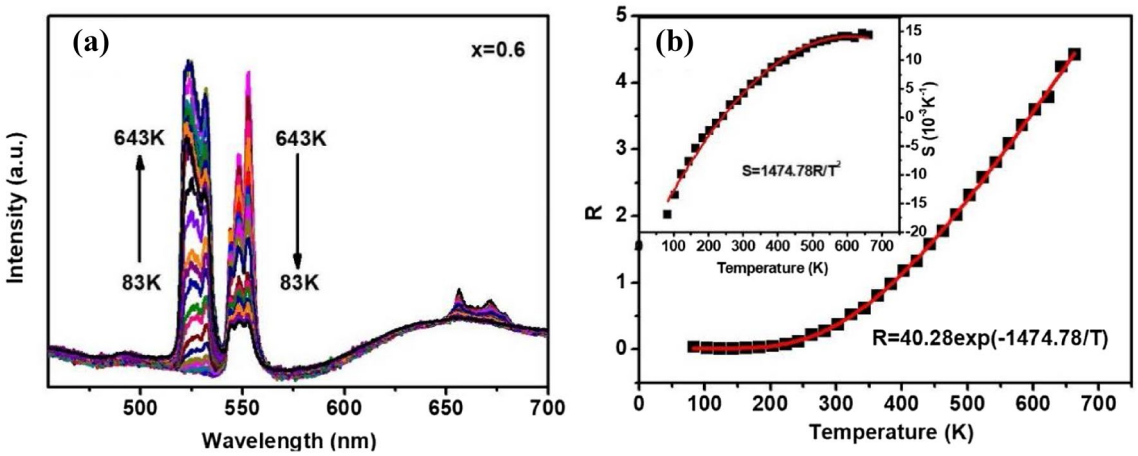

Fig. 4 Temperature sensing properties of 0.6KYW–0.4KW: **a** UCL spectra at different temperature, **b** FIR relative to temperature, the inset shows the temperature dependence of S

the ground state $^4I_{15/2}$ level located at 525 and 553 nm, and a weak red emission band from $^4F_{9/2}$ level to the ground state $^4I_{15/2}$ level located at 660 nm. However, for pure KW sample, there are no red and green emission peaks. For this reason, to simplify the data processing the UCL spectrum of pure KW sample is treated as the background. The common background method is used to deal with the background of xKYW–(1 – x) KW samples. The same operation is also applied in Figs. 3 and 4. Besides, the UCL spectrum of pure KYW has no red emission peak. The Fig. 2b gives the UCL spectra of xKYW–(1 – x) KW samples after background removal. It is obvious that the UCL intensity of multiphase samples are much higher than

Table 2 The optical temperature sensing properties of Er doped and Er/Yb codoped compounds

Materials	Excitation wavelength (nm)	Temperature range (K)	S_{max} (K^{-1})	References
Er/Yb: Y_2O_3	980	93–613	0.0044	[41]
Er/Yb: $Bi_3Ti_{1.5}W_{0.5}O_9$	980	83–483	0.0053	[7]
Er: $Na_{0.5}Bi_{0.5}TiO_3$	980	80–480	0.0053	[42]
Er/Yb: $SrWO_4$	980	95–775	0.0128	[17]
Er/Yb: $SrMoO_4$	980	93–773	0.0128	[43]
Er/Yb: $ZnWO_4$	980	83–583	0.0099	[33]
Er/Yb: $MgWO_4$	980	83–583	0.0081	[15]
Er/Yb: 0.6KYW-0.4KW	980	83–663	0.0147	This work

that of pure phase samples. The optimal luminescent intensity is obtained in 0.6KYW–0.4KW multiphase sample. As observed in the reflectance spectrum in the wavelength region from 200 to 1800 nm shown in Fig. 2c, a series of reflection peaks located at 1521, 980, 803, 656, 548, 490 and 451 nm are detected, which are attributed to the transitions from the $^4I_{5/2}$ ground state to the $^4I_{13/2}$, $^4I_{11/2}$, $^4I_{9/2}$, $^4F_{9/2}$, $^4S_{3/2}$, $^2H_{11/2}$, $^4F_{7/2}$, and $^4F_{3/2}$ excited states of Er^{3+}, respectively. In addition, the observed reflection band at around 980 nm implies that the materials can be excited efficiently by 980 nm laser diode.

Figure 3a, b show the UCL spectra and the corresponding CIE chromaticity diagram of 0.6KYW–0.4KW sample under different pump power from 30 to 70 mW. With the increase of laser power, the UCL intensity of the sample gradually increases, and the emission color gradually moves towards green with high saturation. It indicates that excitation power influences the UCL property of 0.6KYW–0.4KW sample. The Log I versus Log P plot under different pump power is presented in Fig. 3c. For unsaturated UCL process, the number of photons (n) required can be obtained by the formula $I \propto P^n$, where I is the UCL intensity, and P is the pump power [37, 38]. For the above formula, a log transformation is carried out and expressed as $n = \frac{LogI}{LogP}$. The slope (n) of the fitting curve is 1.59, 1.71 and 1.32, respectively, manifesting that two-photon process may be involved in the UC emissions.

To demonstrate the possible application of 0.6KYW–0.4KW multiphase phosphor, the optical temperature sensing performance with the temperature over the range 83–663 K was investigated. The variation of UCL spectra of 0.6KYW–0.4KW sample at different temperature are depicted in Fig. 4a. Note that, the positions of the green and red emission do not change. When the temperature is very low, the green emission located at 525 nm is not obvious. With the increase of temperature, the emission intensity at 525 nm enhances gradually, whereas the emission intensity at 553 nm changes inversely. This should be attributed to the low energy gap between the levels $^2H_{11/2}$ and $^4S_{3/2}$ of Er^{3+} causing the state of $^2H_{11/2}$ populated effectively from $^4S_{3/2}$ by a thermalization process. In addition, the non-radiative relaxation of $^4S_{3/2}$ level is enhanced when the temperature rises. This thermal coupling characteristic enables 0.6KYW–0.4KW multiphase phosphor to have potential applications in temperature sensing. With the thermalization of the population at the levels $^2H_{11/2}$ and $^4S_{3/2}$ of Er^{3+}, the fluorescence intensity ratio (FIR) of I_H/I_S (R) and sensitivity (S) are expressed as follows: $R = I_H/I_S = Ae^{\frac{-\Delta E}{kT}}$, $S = dR/dT = R\frac{\Delta E}{kT^2}$, where A is the pre-exponential factor, ΔE is the energy separation between the $^2H_{11/2}$ and $^4S_{3/2}$ levels, k is the Boltzmann constant, and T is the temperature in Kelvin [6, 39, 40]. The temperature dependence of R and S in the range of 83–663 K (Fig. 4b) shows that the experimental data are properly described by an exponential curve. The coefficient A and calculated ΔE according to fitting curve of the experimental data are 40.28 and 1025 cm^{-1}, respectively. The R and S values both have a clear rise with the increase of temperature. R reaches the maximum value when the temperature approaches the maximal experiment temperature 663 K, while S reaches a maximum value 14.7×10^{-3} K^{-1} at 643 K then decreases slightly.

Compared with other UCL materials given in Table 2, tungstate and molybdate based materials have overwhelming superiority in temperature sensing property. In a broader temperature range, the obtained maximum sensitivity of tungstate and molybdate based materials are much higher. Especially, a highest sensitivity is obtained in the 0.6KYW–0.4KW multiphase material. These results indicate that by material design the temperature sensing properties of $KY(WO_4)_2$–K_2WO_4 multiphase phosphors can be effectively improved. Therefore, 0.6KYW–0.4KW multiphase phosphor with excellent temperature sensing performance has a good prospect in high temperature sensor application.

4 Conclusions

Rare-earth ions Er^{3+}/Yb^{3+} codoped $KY(WO_4)_2$–K_2WO_4 multiphase phosphors were successfully prepared via a conventional solid-sate reaction based on material design. X-ray diffraction pattern confirmed that the multiphase structure was composed of two different monoclinic crystals, $KY(WO_4)_2$ and K_2WO_4. Under a 980 nm excitation, the UCL intensity of multiphase materials was much higher than that of pure phase materials. Furthermore, for the 0.6KYW–0.4KW multiphase material, the maximal sensitivity 14.7×10^{-3} K^{-1} was obtained at 643 K in a broad temperature range from 83 to 663 K. These results indicate that the UCL and temperature sensing properties of $KY(WO_4)_2$–K_2WO_4 multiphase phosphors can be effectively improved by material design. The $KY(WO_4)_2$–K_2WO_4 multiphase phosphors with the excellent UCL and temperature sensing properties are expected to be applied in the field of optical temperature sensor.

Acknowledgements This work was supported by the National Natural Science Foundation of China (Grant No. 51572195). The authors thank all their colleagues for their precious discussions and technical support during the experiments and valuable discussions.

References

1. D.Q. Chen, Z.Y. Wan, Y. Zhou, X.Z. Zhou, Y.L. Yu, J.S. Zhong, M.Y. Ding, Z.G. Ji, ACS Appl. Mater. Interfaces **7**, 19484–19493 (2015)
2. C.D.S. Brites, P.P. Lima, N.J.O. Silva, A. Millán, V.S. Amaral, F. Palacio, L.D. Carlos, Adv. Mater. **22**, 4499–4504 (2010)
3. W. Xu, X. Gao, L. Zheng, P. Wang, Z. Zhang, W. Cao, Appl. Phys. Express **5**, 2201 (2012)
4. D.J. Flannigan, K.S. Suslick, Nature **434**, 52–55 (2005)
5. P.R.N. Childs, J.R. Greenwood, C.A. Long, Rev. Sci. Instrum. **71**, 2959–2978 (2000)
6. A. Pandey, V.K. Rai, Dalton Trans. **42**, 11005–110011 (2013)
7. Y. Zhang, X. Chai, J. Li, X. Wang, Y. Li, X. Yao, J. Alloys Compd. **735**, 473–479 (2017)
8. J.K. Cao, F.F. Hu, L.P. Chen, H. Guo, C. Duan, M. Yin, J. Am. Chem. Soc. **100**, 2108–2115 (2017)
9. D. Chen, S. Liu, X. Li, S. Yuan, P. Huang, J. Eur. Ceram. Soc. **37**, 4939–4945 (2017)
10. Z. Liang, E. Sun, S. Pei, L. Li, F. Qin, Y. Zheng, H. Zhao, Z. Zhang, W. Cao, Opt. Express **24**, 29209–29215 (2016)
11. L. Li, L. Zheng, W. Xu, Z. Liang, Y. Zhou, Z. Zhang, W. Cao, Opt. Lett. **41**, 1458–1461 (2016)
12. X. Cheng, K. Yang, J. Wang, L. Yang, X. Cheng, Opt. Mater. **58**, 449–453 (2016)
13. K. Zheng, Z. Liu, C. Lv, W. Qin, J. Mater. Chem. C **1**, 5502 (2013)
14. Y. Zhang, X. Wang, Y. Li, Y. Li, X. Yao, Opt. Mater. Express **8**, 12 (2018)
15. X. Chai, J. Li, Y. Zhang, X. Wang, Y. Li, X. Yao, RSC Adv. **6**, 64072–64078 (2016)
16. W. Xu, X. Gao, L. Zheng, Z. Zhang, W. Cao, Sens. Actuators B: Chem. **173**, 250–253 (2012)
17. Z. Wei, W. Zheng, Z. Zhu, X. Guo, Chem. Phys. Lett. **651**, 46–49 (2016)
18. M. Anicete-Santos, F.C. Picon, M.T. Escote, E.R. Leite, P.S. Pizani, J.A. Varela, E. Longo, Appl. Phys. Lett. **88**, 30 (2006)
19. S. Han, Y. Wang, Q. Jing, H. Wu, S. Pan, Z. Yang, Dalton Trans. **44**, 5810–5817 (2015)
20. O.A. Savchuk, J.J. Carvajal, C. Cascales, M. Aguilo, F. Diaz, ACS Appl. Mater. Interfaces **8**, 7266–7273 (2016)
21. L. Tong, X. Li, R. Hua, L. Cheng, J. Sun, J. Zhang, S. Xu, H. Zheng, Y. Zhang, B. Chen, Curr. Appl. Phys. **17**, 999–1004 (2017)
22. H. Zheng, B. Chen, H. Yu, J. Zhang, J. Sun, X. Li, M. Sun, B. Tian, S. Fu, H. Zhong, J. Colloid Interface Sci. **420**, 27–34 (2014)
23. J. Xi, M. Ding, J. Dai, Y. Pan, D. Chen, Z. Ji, J. Mater. Sci.: Mater. Electron. **27**, 8254–8270 (2016)
24. B. Tian, B. Chen, Y. Tian, X. Li, J. Zhang, J. Sun, S. Fu, H. Zhong, X. Zhang, H. Yu, Mater. Express **3**, 241–246 (2013)
25. G. Jiang, X. Wei, Y. Chen, C. Duan, M. Yin, B. Yang, W. Cao, Mater. Lett. **143**, 98–100 (2015)
26. G. Liu, L. Fu, Z. Gao, X. Yang, Z. Fu, Z. Wang, Y. Yang, RSC Adv. **5**, 51820–51827 (2015)
27. D. He, C. Guo, S. Jiang, N. Zhang, C. Duan, M. Yin, T. Li, RSC Adv. **5**, 1385–1390 (2015)
28. S. Zhou, X. Wei, X. Li, Y. Chen, C. Duan, M. Yin, Sens. Actuators B: Chem. **246**, 352–357 (2017)
29. F. Hong, B. Yue, Z. Cheng, M. Kunz, B. Chen, H.-K. Mao, Appl. Phys. Lett. **109**, 041907 (2016)
30. P. Du, L. Luo, J.S. Yu, Ceram. Int. **42**, 5635–5641 (2016)
31. W. Xu, Y. Cui, Y. Hu, L. Zheng, Z. Zhang, W. Cao, J. Alloys Compd. **726**, 547–555 (2017)
32. V.K. Rai, A. Pandey, J. Disp. Technol. **12**, 1472–1477 (2017)
33. X. Chai, J. Li, X. Wang, Y. Li, X. Yao, Opt. Express **24**, 22438 (2016)
34. A. Dwivedi, K. Mishra, S.B. Rai, J. Phys. D: Appl. Phys. **50**, 045602 (2017)
35. A.K. Soni, V.K. Rai, S. Kumar, Sens. Actuators B: Chem. **229**, 476–482 (2016)
36. H. Zheng, B. Chen, H. Yu, J. Zhang, J. Sun, X. Li, M. Sun, B. Tian, H. Zhong, S. Fu, R. Hua, H. Xia, RSC Adv. **4**, 47556–47563 (2014)
37. J. Li, X. Chai, X. Wang, C.N. Xu, Y. Gu, H. Zhao, X. Yao, Dalton Trans. **45**, 11733–11741 (2016)
38. Y. Zhang, J. Li, X. Chai, X. Wang, Y. Li, X. Yao, J. Appl. Phys. **121**, 124102 (2017)
39. P.V. dos Santos, M.T. de Araujo, A.S. Gouveia-Neto, J.A. Medeiros Neto, A.S.B. Sombra, Appl. Phys. Lett. **73**, 578–580 (1998)
40. W. Xu, H. Zhao, Y. Li, L. Zheng, Z. Zhang, W. Cao, Sens. Actuators B: Chem. **188**, 1096–1100 (2013)
41. P. Du, L. Luo, Q. Yue, W. Li, Mater. Lett. **143**, 209–211 (2015)
42. S. Wang, H. Zhou, X. Wang, A. Pan, J. Phys. Chem. Solids **98**, 28–31 (2016)
43. P. Du, L. Luo, J.S. Yu, Curr. Appl. Phys. **15**, 46–49 (2015)